

Article

Study on the Influence Law of Ce on Microstructure and High-Temperature Oxidation Resistance of Ti-Al-Si Composite Coating

Siqi Zeng and Faguo Li * 

School of Materials Science and Engineering, Xiangtan University, Xiangtan 411105, China; zengsiqi914201@163.com

* Correspondence: lifaguo@xtu.edu.cn

Abstract: High-temperature titanium alloys are widely used in aerospace hot parts; however, the thermal barrier temperature of 600 °C limits its service temperature. In this paper, a two-step hot-dip plating method is proposed to prepare the composite coating containing Ce on the surface of titanium alloy, which can make the oxidation resistance temperature of titanium alloy reach 800 °C. The microstructure, phase composition, and element distribution of Ce-containing Ti-Al-Si hot-dip coating, Ce-containing Ti-Al-Si pre-oxidation coating and Ce-containing Ti-Al-Si high-temperature oxidation coating were studied. The results showed that the Ti-Al-Si hot-dip coating containing Ce was mainly composed of (Ti,Ce)(Al,Si)₃ alloy phase layer, and the Ti-Al-Si pre-oxidation coating containing Ce was mainly composed of Ti-Al binary system phase layer and dense Al₂O₃ layer rich in CeO₂. Ce in the high-temperature oxidation coating of Ti-Al-Si containing Ce was mainly distributed in Ti₃Al, TiAl, TiAl₃ + Ti₅Si₃ mixed phase layer and Al₂O₃. The addition of Ce could improve the uniformity of composite coating, prevent the spread of cracks, and improve the high-temperature oxidation resistance of Ti-Al-Si coating.

Keywords: Ti-Al-Si composite coating; titanium alloy; Ce; resistance to high-temperature oxidation



Citation: Zeng, S.; Li, F. Study on the Influence Law of Ce on Microstructure and High-Temperature Oxidation Resistance of Ti-Al-Si Composite Coating. *Coatings* **2023**, *13*, 1244. <https://doi.org/10.3390/coatings13071244>

Academic Editor: Elena Villa

Received: 22 June 2023

Revised: 9 July 2023

Accepted: 10 July 2023

Published: 13 July 2023



Copyright: © 2023 by the authors. Licensee MDPI, Basel, Switzerland. This article is an open access article distributed under the terms and conditions of the Creative Commons Attribution (CC BY) license (<https://creativecommons.org/licenses/by/4.0/>).

1. Introduction

Titanium alloys have excellent properties such as high strength, good corrosion resistance, non-magnetic properties, and good welding performance, and are widely used in some cutting-edge fields such as aerospace, military industry, Marine development, and petrochemical industry [1,2]. Aviation materials need to withstand high temperatures, high pressure, high stress, strong corrosion, and other extremely harsh environmental erosion in the service process. High-temperature titanium alloy has excellent mechanical comprehensive properties, which well meet the conditions of aviation materials in high altitude service. High-temperature titanium alloy is widely used in aircraft engines [3–5]. It can greatly reduce their weight and improve their flight speed, for its density is 60% lower than steel and other superalloys, or its weight is 45% lighter than standard low-carbon steel [2].

The initial service temperature of high-temperature titanium alloy was about 350 °C, and it has been continuously developed. At present, the service temperature of high-temperature titanium alloy with relatively perfect technology is about 600 °C [6]. Because titanium alloy had a thermal barrier temperature of 600 °C [7], which meant titanium alloy would undergo secondary oxidation at 600 °C to generate oxides that were no longer dense. Therefore, the use temperature of titanium alloy could not be higher than 600 °C. In order to further improve the service temperature of high-temperature titanium alloys, two solutions were proposed. One was to alloying high-temperature titanium alloys [6,8], which was to add other elements to titanium alloys to modify titanium alloys. This method could improve the service temperature of high-temperature titanium

alloy, but there were great uncertainties. Adding different kinds of alloying elements to high-temperature titanium alloy and conducting different heat treatments would generate different structures, which had a great impact on its mechanical properties. If properly controlled, the performance of titanium alloy would be greatly improved. Conversely, it was also likely to reduce the performance of titanium alloy. Moreover, due to the high dissolved oxygen content of titanium at high temperatures, its surface formed a non-dense porous mixed oxide layer rather than a dense anti-oxidation protective film, which could not effectively prevent further oxidation of the substrate. Therefore, the effect of alloying high-temperature titanium alloys to improve their service temperature was not ideal [5,9,10].

The second solution was to prepare a protective coating on the surface of the titanium alloy [11] without changing the titanium alloy substrate so as to prevent the oxidation of the titanium alloy. Because Ti-Al coating had the advantages of high specific strength, high specific elastic modulus, low density, good oxidation resistance, high corrosion resistance, high creep resistance, and high fatigue resistance, it had great development potential [12]. That was why a layer of Al was initially plated on the surface of titanium alloy to form a TiAl₃-rich layer. TiAl₃ was oxidized into a dense Al₂O₃ [13] film in contact with air, which could well protect the titanium alloy matrix at a temperature lower than 800 °C [14]. However, the aircraft had severe friction with the air flow during high-speed flight, making the actual working temperature of high-temperature titanium alloy higher than 600 °C or even more than 800 °C. Then the Al₂O₃ film could not effectively protect the titanium alloy substrate because a plurality of TiAl phase layers were generated, and the thermal expansion coefficient of the phase layer was not matched with the substrate, resulting in penetration cracks. The addition of the Si element could reduce the number of transverse cracks [3], and compared with the Ti-Al layer, the Ti-Al-Si coating had lower brittleness and better plasticity [15]. When Si was added as an alloying element, the formation of a Si-rich phase could extend the life of the Ti-Al protective layer [16], form an oxygen diffusion barrier to prevent the internal oxidation of Al and Ti, inhibit the formation of harmful nitrides such as TiN and Ti₂AlN, and enhance the adhesion between scale and substrate during the oxidation process [17]. However, due to the high affinity between Ti and Si atoms [18,19], Ti tended to combine with Si to form Ti-Si intermediate phase first and could not form the TiAl₃ phase with good oxidation resistance, which could not protect the substrate.

Therefore, a two-step hot-dip plating method was proposed in this paper, which firstly hot-dip plating Al on the surface of titanium alloy, preferentially formed TiAl₃ phase, and then hot-dip plating alloy liquid containing Si. Referring to the ternary phase diagram of Ti-Al-Si, it could be seen that Si can be solidly dissolved in TiAl₃, replacing some of Al atoms in TiAl₃ to form Ti(Al,Si)₃ secondary solid solution [20]. Compared with other methods for preparing Ti-Al-Si coating, such as the self-generated gradient hot-dipping infiltration (SGHDI) [3,5] and pulsed laser cladding [21,22], the two-step hot-dip plating method could not only better control the content of added Si, inhibit the formation of τ_2 phase but also make the shape of the sample free from the restriction of quartz glass tube, even the sample with complex shape can be hot-dip plating, and the equipment was simple and easy to operate.

The addition of rare earth elements to the alloy can reduce the oxidation rate of the material and increase the binding force of the oxide film [23]. The rare earth elements had purification, modification, and alloying effects [24]. Among them, the Ce element could reduce the oxygen concentration in the alloy [25] to avoid tissue oxidation. At the same time, the formed cerium oxide nanoparticles could refine the grain of titanium alloy and play a role in fine crystal strengthening [26]. Ce element could also inhibit the formation of the τ_2 phase, which might have an adverse effect on the overall oxidation resistance of the coating [3] and improve the high-temperature oxidation resistance of the coating. In summary, the Ce element can improve the performance of the coating from many aspects, for which we chose to add Ce to the Ti-Al-Si coating.

2. Experimental Method and Process

2.1. Coating Preparation

The schematic diagram of experimental process was shown in Figure 1. The wire cut Ti65 (Ti-5.9Al-4.0Sn-3.5Zr-0.3Mo-0.3Nb-2.0Ta-0.4Si-1.0W-0.05C, Dongguan Xinrui gold material Co., LTD., Dongguan, China) samples with length, width, and height of 15 mm, 10 mm, and 3 mm respectively were polished with 400#, 600#, and 800# SiC sandpaper until the surfaces were bright and silver-white. Then the polished Ti65 samples surfaces were cleaned with a metal degreasing agent, then washed with clean water, and put into the ultrasonic cleaning machine (Yu Meng brand, Shenzhen Fangao Microelectronics Co., Ltd., Shenzhen, China) in alcohol to clean and remove water. Finally, put into the drying oven (Xiangtan Mita Electric Furnace Co., Ltd., Xiangtan, China) to dry for use. The purity of 99.999 wt.%Al, purity of 99.999 wt.%Si, high purity Ce were used to prepare a certain quality of pure Al liquid and Al-10 wt.%Si-1 wt.%Ce alloy liquid. The two different melts were placed in two different crucibles and then put into the pit furnace (Dongtai Aozhing Mechanical and Electrical Equipment Factory, Yancheng, China), dissolved by heating at 750 °C. After the solution in the crucible was completely dissolved, argon gas was poured into the pit furnace. Then skimmed off the alumina film on the pure Al liquid and immersed the dried Ti65 sample in the pure Al liquid at 750 °C holding for a certain time for the first hot-dip plating. The oxide film on the Al-10 wt.%Si-1 wt.%Ce alloy liquid was skimmed off, and the sample was extracted from the pure Al liquid. Then it was quickly transferred to the Al-10 wt.%Si-1 wt.%Ce alloy solution for the secondary hot-dip plating. After holding for a certain period of time, the sample was extracted from the alloy solution, and the excess hot-dip solution on the surface was removed. Finally, the sample was quenched and dried.

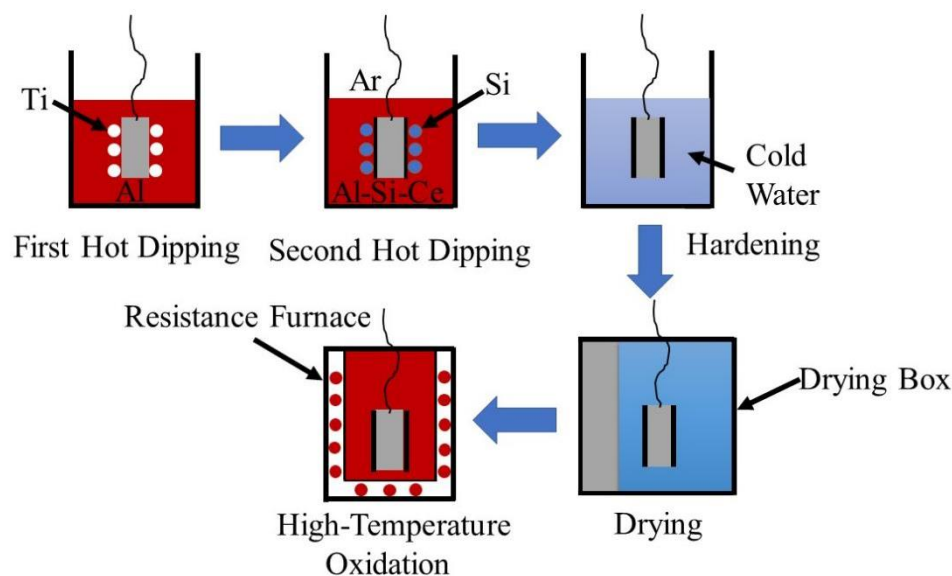


Figure 1. Schematic diagram of experimental process.

2.2. High-Temperature Oxidation Test

By observing the morphology of the coating with different hot-dipping times, the Ti65 sample with dense coating and the moderate thickness of 15 min Al + 15 min Al-10 wt.%Si-1 wt.%Ce was selected for the high-temperature oxidation experiment. The dried samples were put into small corundum crucibles that were washed, dried, and marked, and they were put into a box furnace (Xiangtan Mita Electric Furnace Co., LTD., Xiangtan, China) for pre-oxidation treatment at 500 °C/1 h + 850 °C/2 h, and then took out the crucibles. After they were completely cooled, they were weighed with an electronic balance (Shanghai Huachao Industrial Co., LTD., Shanghai, China) (The samples were heated and weighed in the crucibles to prevent the peeling of the oxide film from affecting the test results). A small crucible was repeatedly weighed 3 times, and the final weight was taken as the average of

the 3 times of weight, which is recorded as the original weight. Then the small crucibles were put into the box furnace for high-temperature oxidation treatment at 800 °C, and the time was recorded. Every day 3 small crucibles were taken out at the same time (the sample in each small crucible had the same process parameters), and then they were weighed after they were completely cooled. Each crucible was weighed 3 times and taken the average, and there were 3 weight values. The increased weight of the sample after high-temperature oxidation was obtained by subtracting the obtained 3 weight values from the weight of the small crucible without high-temperature oxidation and then taking the average value.

2.3. Microstructure Detection

The thickness of the alloy layer was measured by ZEISS optical microscope software. The final coating thickness was obtained from 3 samples with the same process parameters; 10 coating thickness values were measured at different parts of each sample, totaling 30 thickness values, and the average thickness of the coating was taken. Scanning electron microscope (SEM, ZEISS EVO MA10, ZEISS, Jena, Germany) and energy dispersive spectrometer (EDS, OXFORD X-MAXN, ZEISS, Jena, Germany) were used to observe the microstructure of the coating and the surface of the sample, the distribution of each element and they could also determine the content of each element. X-ray diffractometer (XRD, Ultima IV, Rigaku Co., Tokyo, Japan) was used to detect the phase on the surface of high-temperature oxidation-resistant samples.

3. Results and Discussion

3.1. Microstructure Characterization of Coatings

3.1.1. Hot-Dip Coating Tissue

As can be seen from Figure 2, the generated hot-dip coating has obvious delamination. Figure 2a,b are divided into three layers outwards from the substrate: dense alloy layer, loose alloy layer, and liquid layer; Figure 2c,d are divided into two layers outwards from the substrate: dense alloy layer and liquid layer. EDS results (Table 1) show that the content of Al in region 1# is 99.73%, the content of Si is 0.27%, and the atomic percentage of elements in region 2# is Al:Si:Ti = 63.75:9.55:26.57, the Ce content is 0.13%. Combined with Ti-Al-Si ternary phase diagram [27], Ti-Ce phase diagram [28], Al-Ce-Si phase diagram [29] and Al-Ce phase diagram [30], it can be seen that the region of 1# is the Al-Si layer and the region of 2# is the (Ti,Ce)(Al,Si)₃-phase layer. In other words, the (Ti,Ce)(Al,Si)₃ layer and Al-Si layer are successively formed from the substrate after the second hot-dip plating of Al + Al-10 wt.%Si-1 wt.%Ce.

Table 1. EDS data (at.%) and phase components of each phase layer in Figure 2c.

Analysis Region	Al	Si	Ti	Ce	Phase
1#	99.73	0.27	0	0	Al-Si
2#	63.75	9.55	26.57	0.13	(Ti,Ce)(Al,Si) ₃

With the increase in hot-dip plating time of Al-10 wt.%Si-1 wt.%Ce, the (Ti,Ce)(Al,Si)₃ phase layer gradually becomes dense, which is because Ti atoms fully diffuse outward to make up for the vacancy of the loose alloy layer, so the (Ti,Ce)(Al,Si)₃ phase layer becomes denser. The quality of the alloy layer obtained is the best when the hot-dip plating is 15 min Al-10 wt.%Si-1 wt.%Ce. If the hot-dip plating time is increased, although the alloy layer is dense, it is easy to crack.

This method of preparing the coating achieves the purpose of making Al react with the substrate to form the TiAl₃ phase layer first and then let Si atoms and Ce atoms diffuse into it. At the same time, the formation of dense (Ti,Ce)(Al,Si)₃ phase layer is promoted by controlling the hot-dip plating time.

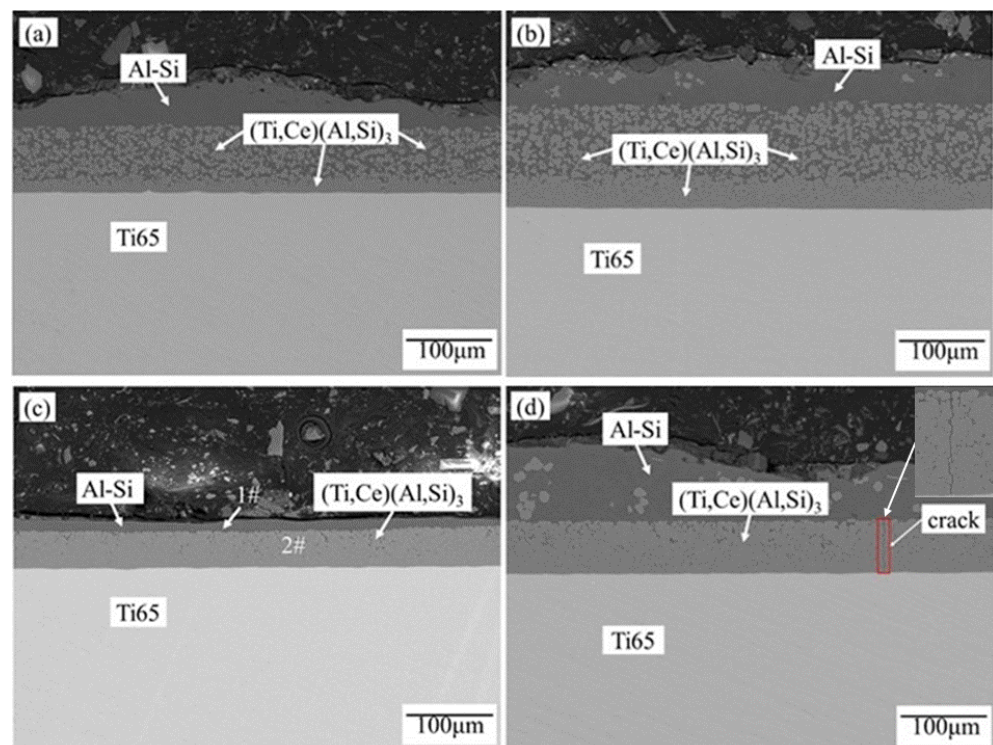


Figure 2. Microstructure of Ti-Al-Si composite coating at 750 °C under different hot-dip plating time, (a) 15 min Al + 5 min (Al-10 wt.%Si-1 wt.%Ce), (b) 15 min Al + 10 min (Al-10 wt.%Si-1 wt.%Ce), (c) 15 min Al + 15 min (Al-10 wt.%Si-1 wt.%Ce), (d) 15 min Al + 20 min (Al-10 wt.%Si-1 wt.%Ce).

3.1.2. Growth Kinetics of Coatings

Analysis of the growth kinetics of $(\text{Ti,Ce})(\text{Al,Si})_3$ alloy layer is helpful in understanding the formation mechanism of the $(\text{Ti,Ce})(\text{Al,Si})_3$ alloy layer. In addition, the $(\text{Ti,Ce})(\text{Al,Si})_3$ alloy layer is the key coating to resist high-temperature oxidation of titanium alloy, so it is necessary to analyze the growth kinetics of the $(\text{Ti,Ce})(\text{Al,Si})_3$ alloy layer. There is an empirical formula [31]:

$$\delta_x = kt^n \quad (1)$$

where δ is the alloy layer thickness (μm), x is the fixed hot-dip plating time (min), in Figure 3a, x is the time of hot dip plating Al + Al-Si-Ce, in Figure 3b, x is the time of hot dip plating pure Al, t is the hot immersion time (min), k is the rate constant, n is the kinetic index, and the kinetic index $n \leq 0.5$ is the diffusion-controlled growth, $n > 0.5$ is interfacial controlled growth (reaction controlled growth).

The kinetic index $n > 0.5$ in the fitting formula of Figure 3a indicates that hot-dip plating Al controls the growth of $(\text{Ti,Ce})(\text{Al,Si})_3$ alloy layer by the reaction. In the fitting formula of Figure 3b the kinetic index $n \leq 0.5$ indicates that hot-dip plating of Al-Si-Ce controls the growth of $(\text{Ti,Ce})(\text{Al,Si})_3$ alloy layer through diffusion.

The results show that the growth of $(\text{Ti,Ce})(\text{Al,Si})_3$ alloy layer is affected by two hot-dipping. It can be seen from the fitting curve that with the increase in hot-dipping plating time, the alloy layer thickness shows an increasing trend as a whole. Compared with the steepness of the curves in Figure 3a,b, it can be seen that the hot-dipping Al plating time has a greater impact on the coating thickness, which means the coating thickness increases more with the increase in the hot-dipping Al plating time.

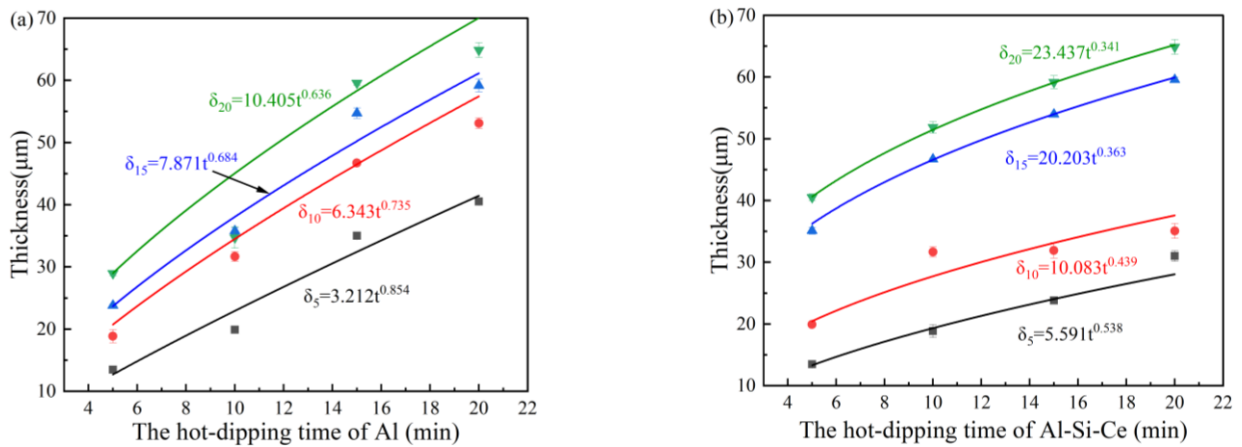


Figure 3. Growth kinetics curve of (Ti,Ce)(Al,Si)₃ alloy layer, (a) the variation curve of coating thickness with hot-dip plating Al time, (b) the variation curve of coating thickness with hot-dip plating Al-Si-Ce time.

3.2. Microstructure Characterization of High-Temperature Pre-Oxidation Coating

It can be seen from Figure 4 that Ti65 alloy, after pre-oxidation, the previous single (Ti,Ce)(Al,Si)₃ alloy layer changes into a multiphase layer structure. Under high temperatures, the Al atom further diffuses towards the substrate, and the Ti atom also diffuses outwards, and the two atoms combine to form a more dense TiAl alloy layer. The O atom reacts with the Al atom in the outermost (Ti,Ce)(Al,Si)₃ alloy layer to form dense Al₂O₃ and reacts with the Ce atom to form CeO₂. According to EDS data (Table 2), and Ti-Al-Si ternary phase diagram [27], Ti-Ce phase diagram [28], Al-Ce-Si phase diagram [29] and Al-Ce phase diagram [30], Ti₃Al layer, TiAl layer, TiAl₂ layer, and CeO₂-rich Al₂O₃ + (Ti,Ce)(Al,Si)₃ mixed-phase layer are formed outward from the substrate successively. Ce atoms have diffused inward from the outermost (Ti,Ce)(Al,Si)₃ alloy layer into the newly formed Ti-Al phase layers.

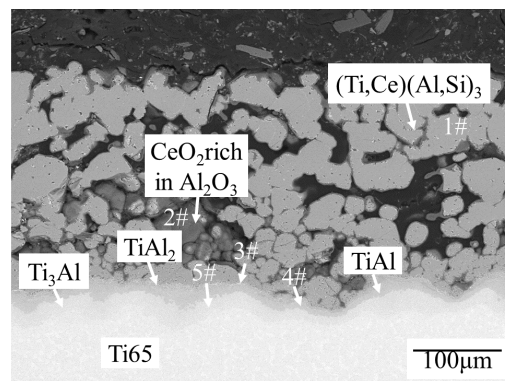


Figure 4. Microstructure of the coating after hot-dipping Al + 15 min (Al-10 wt.%Si-1 wt.%Ce) and preoxidation at 500 °C/1 h + 850 °C/2 h.

Table 2. EDS data (at.%) and phase components of each phase layer in Figure 4.

Analysis Region	O	Al	Si	Ti	Ce	Phase
1#	0	67.51	4.77	27.63	0.09	(Ti,Ce)(Al,Si) ₃
2#	55.55	41.76	0	2.57	0.12	Al ₂ O ₃ + CeO ₂
3#	0	64.24	2.13	33.57	0.06	TiAl ₂
4#	0	41.43	2.28	55.90	0.39	TiAl
5#	0	20.90	0	78.88	0.22	Ti ₃ Al

3.3. High-Temperature Oxidation Properties of Coatings

3.3.1. High-Temperature Oxidation Coating Morphology

It can be seen from Figure 5a that the coating oxidized 23 days at 800 °C is still relatively uniform and dense. Combined with the XRD pattern in Figure 6, EDS data analysis in Table 3, Ti-Al-Si terpolymer phase diagram [27], Ti-Ce phase diagram [28], Al-Ce-Si phase diagram [29], and Al-Ce phase diagram [30], it can be seen that after high-temperature oxidation, not only TiAl phase but also Ti₅Si₃ phase is formed. That is, with the increase in high-temperature oxidation time, Si atoms in the (Ti,Ce)(Al,Si)₃ phase also diffuse to the substrate. However, due to the obstruction of the Ti₃Al layer and TiAl layer, Si atoms cannot be directly combined with the substrate. EDS data show that after high-temperature oxidation, the Ti₃Al layer, TiAl layer, TiAl₃ + Ti₅Si₃ mixed-phase layer, and CeO₂-rich Al₂O₃ + (Ti,Ce)(Al,Si)₃ mixed-phase layer are formed outwards from the substrate.

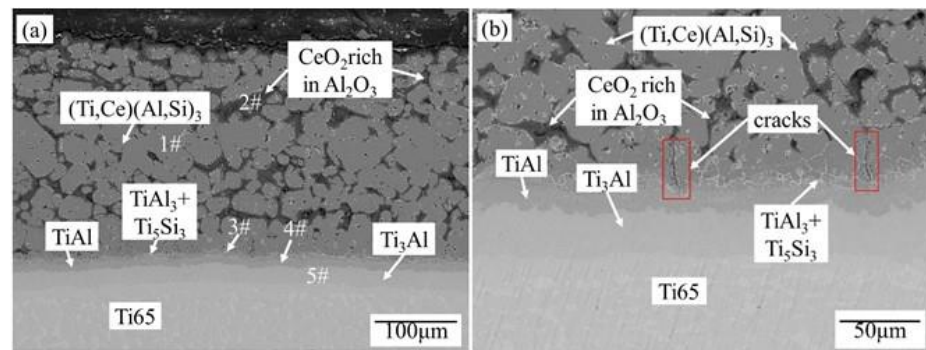


Figure 5. Microstructure of Ti65 alloy oxidized coating at high temperature after 15 min Al + 15 min (Al-10 wt.%Si-1 wt.%Ce), (a) 23 days, (b) 14 days.

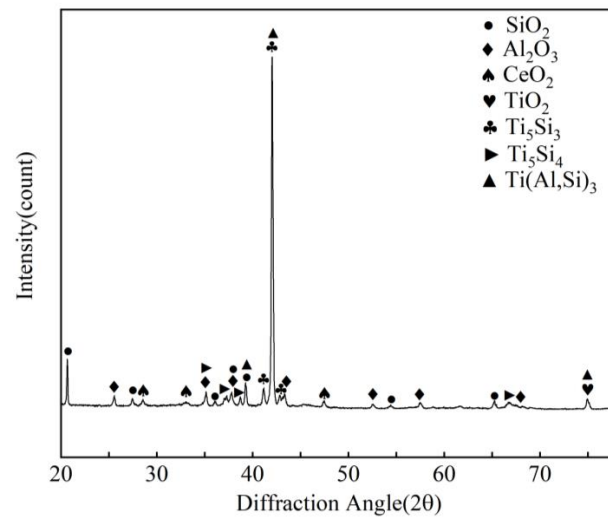


Figure 6. XRD pattern of Ti-Al-Si composite coating at 800 °C for 23 days oxidation.

Table 3. EDS data (at.%) and phase components of each phase layer in Figure 5a.

Analysis Region	O	Al	Si	Ti	Ce	Phase
1#	0	66.37	3.78	29.74	0.11	(Ti,Ce)(Al,Si) ₃
2#	59.96	37.59	0	2.30	0.15	Al ₂ O ₃ + CeO ₂
3#	0	36.22	20.36	43.35	0.07	TiAl ₃ + Ti ₅ Si ₃
4#	0	37.55	3.93	58.28	0.24	TiAl
5#	0	21.18	0	78.61	0.21	Ti ₃ Al

3.3.2. High-Temperature Oxidation Kinetics

The fitting formula of the high-temperature oxidation weight gain curve of the substrate at 800 °C is as follows:

$$\Delta m' = 0.544t^{0.932} \quad (2)$$

where Δm is the oxidation weight gain of the coated sample (mg/cm^2), $\Delta m'$ is the oxidation weight gain of the substrate (mg/cm^2), and t is the oxidation time (h).

After hot-dip plating 15 min Al + 15 min Al-10 wt.%Si-1 wt.%Ce on Ti65 alloy, the fitting formula of the high-temperature oxidation weight gain curve at 800 °C is as follows:

$$\Delta m = 0.963t^{0.328} \quad (3)$$

After hot plating Al on Ti-6Al-4V alloy, the fitting formula of the high-temperature oxidation weight gain curve at 800 °C is as follows [32]:

$$\Delta m = 0.582t^{0.5} \quad (4)$$

After hot impregnation of Ti-Al-Si on Ti-6Al-4V alloy, the fitting formula of the high-temperature oxidation weight gain curve at 800 °C is as follows [3,5]:

$$\Delta m = 0.624t^{0.5} \quad (5)$$

It can be seen from the high-temperature oxidation weight gain curve (Figure 7) that the weight of uncoated Ti65 alloy and coated Ti65 alloy increases with the increase in high-temperature oxidation time under the condition of high-temperature oxidation at 800 °C. This is because, during the high-temperature oxidation process, the O atom diffuses into the coating and generates CeO_2 , Al_2O_3 , and other oxides. Therefore, the weight of the alloy is increased. Comparing the two weight gain curves and Formulas (2)–(5), it is obvious that the weight gain rate of Ti65 substrate is the fastest and the weight gain is the most, while the sample of hot-dip plating Al + Al-Si-Ce has the slowest oxidation weight gain rate and the least weight increase. $(2)/(3) = 0.565t^{0.604}$, which indicates the excellent property of the coating becomes more obvious with the increase in high-temperature oxidation time. Therefore, the Ti-Al-Si coating with Ce element can greatly improve the high-temperature oxidation resistance of Ti65 alloy.

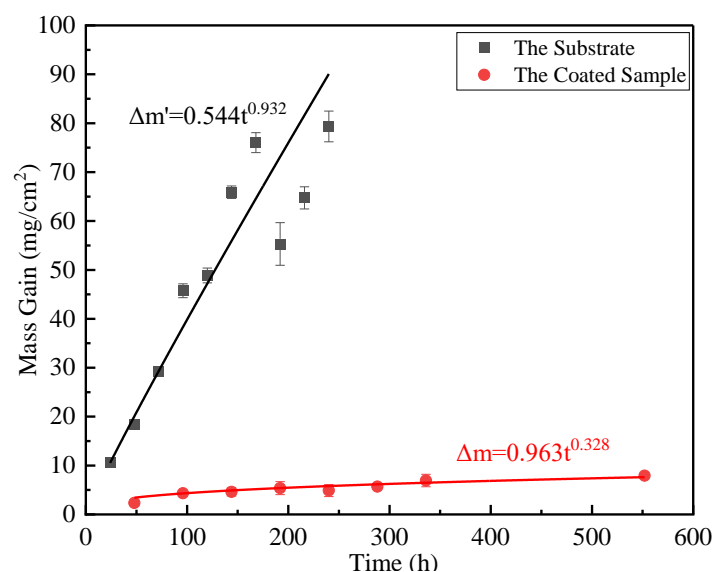


Figure 7. High-temperature oxidation weight gain curves of substrate and sample.

3.3.3. Crack

Figure 5b shows the coating structure of Ti65 alloy after hot-dip plating 15 min Al + 15 min Al-10 wt.%Si-1 wt.%Ce for 14 days. Obvious longitudinal cracks appear in the coating, but the cracks do not extend to the substrate but stop at the $\text{TiAl}_3 + \text{Ti}_5\text{Si}_3$ mixed-phase layer, indicating that the dense $\text{TiAl}_3 + \text{Ti}_5\text{Si}_3$ mixed-phase layer, TiAl layer, and Ti_3Al layer hinder the crack propagation, thus blocking the path of O_2 entering the substrate.

3.4. Mechanism of Coating Formation and Resistance to High-Temperature Oxidation

3.4.1. The Mechanism of Coating Formation

The Ti-Al binary system phase formed during hot-dip plating may be TiAl_3 , TiAl_2 , TiAl, and Ti_3Al , and their Gibbs free energies are as follows (Figure 8) [33]:

$$\Delta G_f (\text{TiAl}_3) = -40,349.6 + 10.36525T(\text{K}) \quad (6)$$

$$\Delta G_f (\text{TiAl}_2) = -43,858.4 + 11.02077T(\text{K}) \quad (7)$$

$$\Delta G_f (\text{TiAl}) = -37,445.1 + 16.79376T(\text{K}) \quad (8)$$

$$\Delta G_f (\text{Ti}_3\text{Al}) = -29,633.6 + 6.70801T(\text{K}) \quad (9)$$

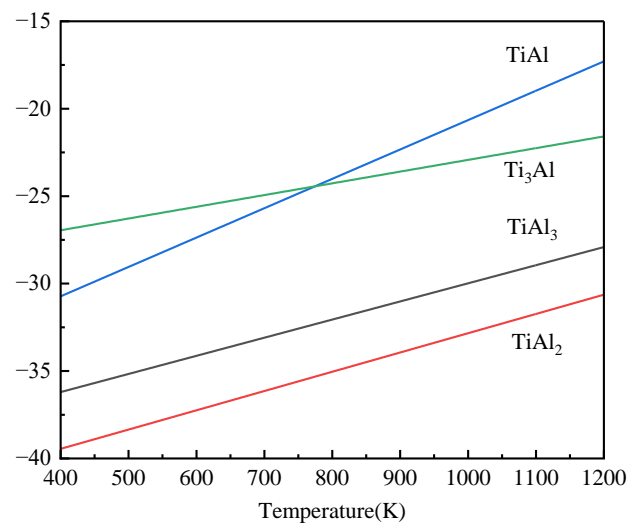
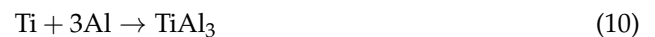


Figure 8. Gibbs free energy curves of some Ti-Al binary system phases with temperature.

Although TiAl_2 has the lowest Gibbs free energy of formation, it can only nucleate at the TiAl interface [14]. The activation energies of intermetallic compounds in the Ti-Al system are $Q_{\text{Ti}_3\text{Al}} > Q_{\text{TiAl}_2} > Q_{\text{TiAl}} > Q_{\text{TiAl}_3}$ [5], so Ti65 alloy reacts with pure Al to preferentially form TiAl_3 layer and then reacts with Al-10 wt.%Si-1 wt.%Ce alloy liquid. Because Si atoms tend to bond with Ti65 alloy substrate, Si atoms will enter the coating to replace Al atoms in the TiAl_3 layer. Due to the high activity of the Ce element, Ce atoms can replace Ti atoms [34,35] and finally form $(\text{Ti,Ce})(\text{Al,Si})_3$ composite phase layer, and the excess alloy liquid forms the Al-Si layer. The schematic diagram of formation mechanism of alloy layer was shown in Figure 9. The reaction formulas are as follows:



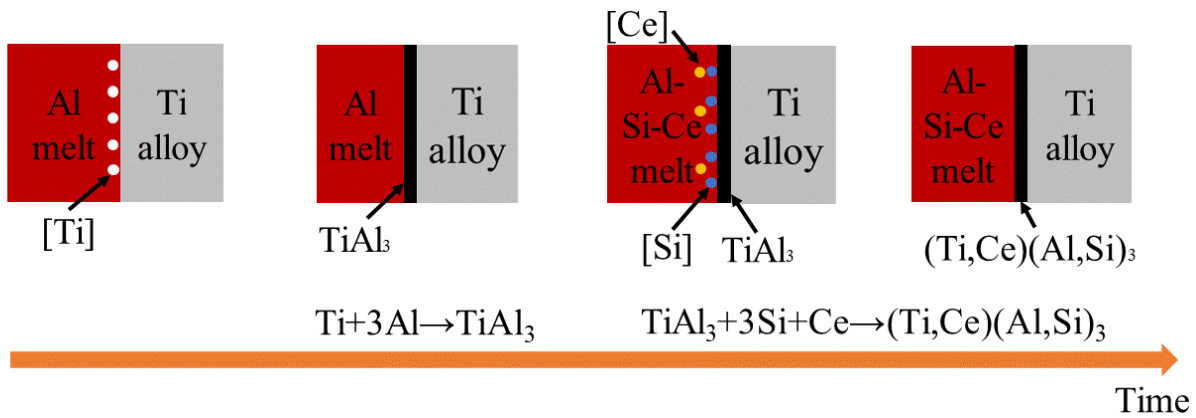


Figure 9. Schematic diagram of formation mechanism of alloy layer.

3.4.2. High-Temperature Resistance Mechanism

The schematic diagram of high-temperature oxidation mechanism was shown in Figure 10. After high-temperature oxidation, the coating changes from a single $(\text{Ti,Ce})(\text{Al,Si})_3$ alloy layer into Ti_3Al layer, TiAl layer, $\text{TiAl}_3 + \text{Ti}_5\text{Si}_3$ mixed-phase layer, and CeO_2 -rich $\text{Al}_2\text{O}_3 + (\text{Ti,Ce})(\text{Al,Si})_3$ mixed-phase layer. This indicates that with the increase in high-temperature oxidation time, all the excess Al-Si layers are consumed, forming $(\text{Ti,Ce})(\text{Al,Si})_3$ phases and Ti, Al, Si atoms are diffused with each other, forming Ti-Si binary system phases and multiple Ti-Al binary system phases. The increase in temperature can accelerate the diffusion of atoms, in which the formation of intermetallic bonds is faster. Therefore, the coating near the substrate is the Ti-Al layer [36]. In the process of high-temperature oxidation, O_2 reacts with Al atoms in $(\text{Ti,Ce})(\text{Al,Si})_3$ to form dense Al_2O_3 . As rare earth elements have a strong affinity with O and S [37], Ce tends to combine with Al_2O_3 in the coating to form a CeO_2 -rich Al_2O_3 phase. The doping of CeO_2 helps to improve the uniformity and crystallinity of the composite coating, thus improving the high-temperature oxidation resistance of the Al_2O_3 coating [38]. The formed dense $\text{TiAl}_3 + \text{Ti}_5\text{Si}_3$ mixed-phase layer, TiAl layer, and Ti_3Al layer can prevent crack extension because the increase in Al content in the TiAl compound and the increase in thermal expansion coefficient, making the newly formed TiAl and TiAl_3 reduce the mismatch of thermal expansion coefficient between the coating and the base alloy [14]. At the same time, the Ce element diffuse into $\text{TiAl}_3 + \text{Ti}_5\text{Si}_3$ mixed-phase layer, TiAl layer, and Ti_3Al layer. The steel containing rare earth has a low high Angle boundary and mean crystal orientation error. It can effectively prevent crack propagation [39], so cracks in the coating cannot spread to the $\text{TiAl}_3 + \text{Ti}_5\text{Si}_3$ mixed-phase layer, TiAl layer, and Ti_3Al layer.

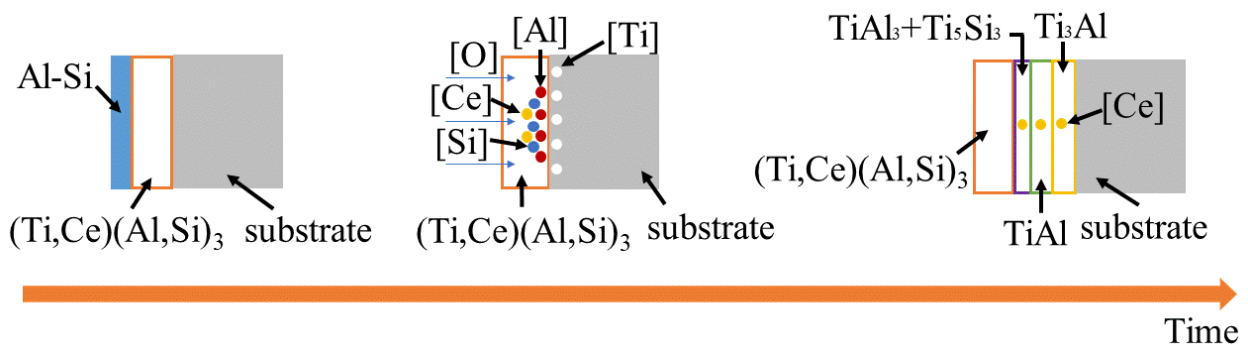


Figure 10. Schematic diagram of high-temperature oxidation mechanism.

In the process of high-temperature oxidation, a dense continuous CeO_2 -rich Al_2O_3 oxide film is formed to prevent the diffusion of O atoms into the substrate. A $\text{TiAl}_3 + \text{Ti}_5\text{Si}_3$ mixed-phase layer, a TiAl layer, and a Ti_3Al layer containing Ce are formed to prevent the

propagation of cracks, thus preventing the diffusion of O atoms. The reaction equations are as follows:



4. Conclusions

In this study, Ti-Al-Si composite coating containing Ce was prepared on Ti65 alloy by a two-step hot-dip plating method. The addition of Ce element improved the high-temperature oxidation resistance of Ti-Al-Si composite coating. The main conclusions are as follows:

- (1) The two-step hot-dip coating is mainly composed of (Ti,Ce)(Al,Si)₃ alloy layer. With the increase in the second step hot-dip plating time of Al-10 wt.%Si-1 wt.%Ce, the alloy layer gradually becomes dense.
- (2) The growth kinetic law of the hot-dip plating coating is that the coating thickness generally increases with the increase in the hot-dip plating time (the first or second step), and the influence of the first step hot-dip plating time on the coating thickness is greater.
- (3) In the process of pre-oxidation, the substrate reacts with (Ti,Ce)(Al,Si)₃ alloy layers to form multiple Ti-Al binary system phase layers. From the substrate, Ti₃Al layer, TiAl layer, TiAl₂ layer, and CeO₂-rich Al₂O₃ + (Ti,Ce)(Al,Si)₃ mixed-phase layers are formed successively.
- (4) After high-temperature oxidation, the Ti₃Al layer, TiAl layer, TiAl₃ + Ti₅Si₃ mixed-phase layer, and CeO₂-rich Al₂O₃ + (Ti,Ce)(Al,Si)₃ mixed-phase layer are formed outward from the substrate in turn. The dense TiAl₃ + Ti₅Si₃ mixed-phase layer containing the Ce element, the dense TiAl layer, and the dense Ti₃Al layer can be obtained to prevent crack propagation to the substrate.
- (5) During the high-temperature oxidation process, the Ce element combines with Al₂O₃ in the form of CeO₂, which improves the Al₂O₃ layer's high-temperature oxidation resistance. After 23 days oxidation at a high temperature, the weight gain of the substrate is 26 times that of the coated sample.

Author Contributions: Investigation, data curation, and writing—original draft, S.Z.; supervision, project administration, funding acquisition, methodology, and writing—reviewed, F.L. All authors have read and agreed to the published version of the manuscript.

Funding: This research was funded by the Science and Technology Project of the Education Department of Hunan Province (No. 22A0100), Hunan Provincial Natural Science Foundation of China (No. 2021JJ30672), and the College Students' Innovation and Entrepreneurship Training Program of Xiangtan University.

Institutional Review Board Statement: Not applicable.

Informed Consent Statement: Not applicable.

Data Availability Statement: Not applicable.

Acknowledgments: The authors gratefully acknowledge the support provided by Materials Intelligent Design College Students' Innovation and Entrepreneurship Education Center, Xiangtan University, Xiangtan, Hunan.

Conflicts of Interest: The authors declare no conflict of interest.

References

1. Zhao, Q.Y.; Sun, Q.Y.; Xin, S.W.; Chen, Y.N.; Wu, C.; Wang, H.; Xu, J.W.; Wan, M.P.; Zeng, W.D.; Zhao, Y.Q. High-strength titanium alloys for aerospace engineering applications: A review on melting-forging process. *Mater. Sci. Eng. A* **2022**, *845*, 143260. [[CrossRef](#)]
2. Pushp, P.; Dasharath, S.M.; Arati, C. Classification and applications of titanium and its alloys. *Mater. Today* **2022**, *54*, 537–542. [[CrossRef](#)]
3. Wang, Z.H.; Li, F.G.; Hu, X.Y.; He, W.; Liu, Z.; Tan, Y. Preparation of Ti-Al-Si Gradient Coating Based on Silicon Concentration Gradient and Added-Ce. *Coatings* **2022**, *12*, 683. [[CrossRef](#)]
4. Luo, S.Y.; Yao, J.; Zou, G.M.; Li, J.; Jiang, J.; Yu, F.P. Transformation characteristics of temperature and phases within Ti-6Al-4V aeroengine drum in hot forging and air cooling procedures. *J. Mater. Res. Technol.* **2020**, *9*, 8235–8244. [[CrossRef](#)]
5. Hu, X.Y.; Li, F.G.; Shi, D.M.; Xie, Y.; Li, Z.; Yin, F.C. A design of self-generated Ti–Al–Si gradient coatings on Ti–6Al–4V alloy based on silicon concentration gradient. *J. Alloys Compd.* **2020**, *830*, 154670. [[CrossRef](#)]
6. Wen, P.C.; Yuan, L.J.; Tao, R.; Li, J.; Li, D. First-principles investigation of interaction between surface oxygen and other alloy atoms in α -Ti (0001) for designing high-temperature titanium alloy. *Appl. Surf. Sci.* **2022**, *604*, 154535. [[CrossRef](#)]
7. Zhao, E.T.; Sun, S.C.; Zhang, Y. Recent advances in silicon containing high temperature titanium alloys. *J. Mater. Res. Technol.* **2021**, *14*, 3029–3042. [[CrossRef](#)]
8. Tian, Y.S.; Zhang, Q.Y.; Wang, D.Y. Study on the microstructures and properties of the boride layers laser fabricated on Ti-6Al-4V alloy. *J. Mater. Process. Technol.* **2009**, *209*, 2887–2891. [[CrossRef](#)]
9. Zheng, N.; Fischer, W.; Griibrneier, H.; Shernet, V.; Qiradakkars, W.J. The significance of sub-surface depletion layer composition for the oxidation behavior of g-titanium aluminides. *Scr. Metall. Mater.* **1995**, *33*, 47–53. [[CrossRef](#)]
10. Rakowski, J.M.; Pettit, F.S.; Meier, G.H.; Dettenwanger, F.; Schumann, E.; Ruhle, M. The effect of nitrogen on the oxidation of g-TiAl. *Scripta Metall. Mater.* **1995**, *33*, 997–1003. [[CrossRef](#)]
11. Xiang, J.Y.; Xie, F.Q.; Wu, X.Q.; Wang, S.Q.; Li, L. Hot corrosion behavior of a Si Y co-deposition coating on a Ti₂AlNb based alloy in NaCl-Na₂SO₄ mixture. *Surf. Coat. Technol.* **2021**, *419*, 127282. [[CrossRef](#)]
12. Pan, C.G.; Fang, C.J.; Shi, J.; Ma, K.J.; Yang, H.; He, P. Synthesis and properties of Ti-Al coating by high-frequency induction heated combustion. *J. Alloys Compd.* **2023**, *939*, 168739. [[CrossRef](#)]
13. Kuzminova, Y.O.; Firsov, D.G.; Shibalova, A.A.; Evlashin, S.A.; Shishkovsky, I.V.; Dautov, S.S. The oxidation behavior of the CrFeCoNiAl(x) (x = 0, 1.0, and 5.0 wt%) high-entropy alloy synthesized with Al elemental powder via powder bed fusion technique at high temperatures. *Micron* **2023**, *166*, 103399. [[CrossRef](#)]
14. Zhang, Z.G.; Peng, Y.P.; Mao, Y.L.; Pang, C.J.; Lu, L.Y. Effect of hot-dip aluminizing on the oxidation resistance of Ti-6Al-4V alloy at high temperatures. *Corros. Sci.* **2012**, *55*, 187–193. [[CrossRef](#)]
15. Sui, X.M.; Lu, J.; Wei, D.Q.; Zhang, L.; Wang, R.; Zhao, W.; Zhang, W.P. Unveiling the influence of TiN on the microstructure and high-temperature oxidation behavior of Ti-Al-Cr composite coating. *Corros. Sci.* **2022**, *206*, 110539. [[CrossRef](#)]
16. Cammarota, G.P.; Casagrande, A.; Sambogna, G. Effect of Ni, Si and Cr in the structural formation of diffusion aluminide coatings on commercial-purity titanium. *Surf. Coat. Technol.* **2006**, *201*, 230–242. [[CrossRef](#)]
17. Oukati Sadeq, F.; Sharifitabar, M.; Shafiee Afarani, M. Synthesis of Ti-Si-Al coatings on the surface of Ti-6Al-4V alloy via hot dip siliconizing route. *Surf. Coat. Technol.* **2018**, *337*, 349–356. [[CrossRef](#)]
18. Crespo-Villegas, J.; Cavarroc, M.; Knittel, S.; Martinu, L.; Klemberg-Sapieha, J.E. Protective Ti_xSi_y coatings for enhanced oxidation resistance of the γ -TiAl alloy at 900 °C. *Surf. Coat. Technol.* **2022**, *430*, 127936. [[CrossRef](#)]
19. Chen, C.; Feng, X.M.; Shen, Y.F. Oxidation behavior of a high Si content Al-Si composite coating fabricated on Ti-6Al-4V substrate by mechanical alloying method. *J. Alloys Compd.* **2017**, *701*, 27–36. [[CrossRef](#)]
20. Li, X.T.; Huang, L.J.; Jiang, S.; Gao, Y.N.; An, Q.; Wang, S.; Zhang, R.; Geng, L. Microstructure and super oxidation resistance of the network structured Ti-Al-Si coating. *J. Alloys Compd.* **2019**, *807*, 151679. [[CrossRef](#)]
21. Zhang, S.Y.; Han, B.; Zhang, T.M.; Chen, Y.H.; Xie, J.L.; Shen, Y.; Huang, L.; Qin, X.W.; Wu, Y.B.; Pu, K.J. High-temperature solid particle erosion characteristics and damage mechanism of Al_xCoCrFeNiSi high-entropy alloy coatings prepared by laser cladding. *Intermetallics* **2023**, *159*, 107939. [[CrossRef](#)]
22. Li, Z.H.; Chai, L.J.; Qi, L.; Wang, Y.Y.; Liu, Y.Z.; Yang, T.; Wang, H.; Guo, N.; Zhao, Y.X. Laser-cladded Al-Cr-Ti ternary alloy coatings on Ti-4Al-2V alloy: Specific microstructure and enhanced surface performance. *Surf. Coat. Technol.* **2023**, *452*, 129073. [[CrossRef](#)]
23. Du, X.J.; Ma, X.Y.; Ding, X.; Zhang, W.; He, Y.Z. Enhanced high-temperature oxidation resistance of low-cost Fe-Cr-Ni medium entropy alloy by Ce-adulterated. *J. Mater. Res. Technol.* **2022**, *16*, 1466–1477. [[CrossRef](#)]
24. He, Y.M.; Lu, C.Y.; Ni, C.Y.; Chen, Q.X.; Zheng, W.J.; Wang, D.H.; Wei, L.F.; Wang, L.M.; Sun, Y.; Zou, H.; et al. Tailoring microstructure and mechanical performance of the TC4 titanium alloy brazed joint through doping rare-earth element Dy into Ti-Cu-Ni filler alloy. *J. Manuf. Process.* **2020**, *50*, 255–265. [[CrossRef](#)]
25. Xue, X.Y.; Ma, C.M.; Liu, Y.R.; Wang, H.; Chen, Q.J. Impacts of Ce dopants on the hydrogen storage performance of Ti-Cr-V alloys. *J. Alloys Compd.* **2023**, *934*, 167947. [[CrossRef](#)]
26. Xu, Y.; Liu, Z.; Zhu, X.H.; Jiang, Z.L.; Chen, H.; Wang, N. Effect of rare earth Ce addition on microstructure and mechanical properties of titanium alloy Ti-6Al-4V. *Mater. Lett.* **2023**, *330*, 133244. [[CrossRef](#)]

27. Li, Z.; Liao, C.L.; Liu, Y.X.; Wang, X.M.; Wu, Y.; Zhao, M.X.; Long, Z.H.; Yin, F.C. 700 °C Isothermal Section of the Al-Ti-Si Ternary Phase Diagram. *J. Phase Equilibria Diffus.* **2014**, *35*, 564–574. [[CrossRef](#)]
28. Yao, B.; Hu, B.; Zhang, A.A.; Zhao, J.R.; Wang, J.; Du, Y. Thermodynamic Assessment of the Ti-RE (RE = Ce, Er, Tm, Y) Binary Systems. *J. Phase Equilibria Diffus.* **2018**, *39*, 44–50. [[CrossRef](#)]
29. Raghavan, V. Al-Ce-Si (Aluminum-Cerium-Silicon). *J. Phase Equilibria Diffus.* **2007**, *28*, 456–458. [[CrossRef](#)]
30. Okamoto, H. Al-Ce (Aluminum-Cerium). *J. Phase Equilibria Diffus.* **2011**, *32*, 392–393. [[CrossRef](#)]
31. Marder, A.R. The metallurgy of zinc-coated steel. *Prog. Mater. Sci.* **2000**, *45*, 191–271. [[CrossRef](#)]
32. Jeng, S.-C. Oxidation behavior and microstructural evolution of hot-dipped aluminum coating on Ti-6Al-4V alloy at 800 °C. *Surf. Coat. Technol.* **2013**, *235*, 867–874. [[CrossRef](#)]
33. Kattner, U.R.; Lin, J.C.; Chang, Y.A. Thermodynamic Assessment and Calculation of the Ti-Al System. *Metall. Trans. A* **1992**, *23*, 2081–2090. [[CrossRef](#)]
34. Niu, G.D.; Wang, J.; Li, J.P.; Ye, J.W.; Mao, J. Characterization of in-situ reinforced (Al,Si)₃(Ti,Ce) precipitates in T6 treated A356-0.3wt.%Ce-1.5vol.%TiCN composite and its effects on mechanical properties. *Mater. Charact.* **2022**, *185*, 111756. [[CrossRef](#)]
35. Fan, L.; Liu, M.; Wang, Y.L.; Cui, H.B.; Ren, X.D.; Xin, B. Microstructure, mechanical properties and corrosion behavior of Ce doped TiN films. *Appl. Surf. Sci.* **2022**, *575*, 151770. [[CrossRef](#)]
36. Zhang, L.; Xiong, D.J.; Su, Z.L.; Li, J.F.; Yin, L.M.; Yao, Z.X.; Wang, G.; Zhang, L.P.; Zhang, H.H. Molecular dynamics simulation and experimental study of tin growth in SAC lead-free micro solder joints under thermo-mechanical-electrical coupling. *Mater. Today Commun.* **2022**, *33*, 104301. [[CrossRef](#)]
37. Cheng, W.S.; Song, B.; Mao, J.H. Effect of Ce content on the hydrogen induced cracking of X80 pipeline steel. *Int. J. Hydrogen Energy* **2023**, *48*, 15303–15316. [[CrossRef](#)]
38. Wang, S.Q.; Xie, F.Q.; Wu, X.Q.; Chen, L.Y. CeO₂ doped Al₂O₃ composite ceramic coatings fabricated on γ-TiAl alloys via cathodic plasma electrolytic deposition. *J. Alloys Compd.* **2019**, *788*, 632–638. [[CrossRef](#)]
39. Das, A.K. Effect of rare earth oxide additive in coating deposited by laser cladding: A review. *Mater. Today Proc.* **2022**, *52*, 1558–1564. [[CrossRef](#)]

Disclaimer/Publisher's Note: The statements, opinions and data contained in all publications are solely those of the individual author(s) and contributor(s) and not of MDPI and/or the editor(s). MDPI and/or the editor(s) disclaim responsibility for any injury to people or property resulting from any ideas, methods, instructions or products referred to in the content.